Chiang Mai J. Sci. 2018; 45(4) : 1827-1834
http://epg.science.cmu.ac.th/ejournal/
Contributed Paper

Ethanol Sensors Fabricated from PdO/WO_3 Nanorods

Sathukarn Kabcum [a, b], Duangdao. Channei [c], Adisorn Tuantranont [d], Anurat Wisitsoraat [d], Chaikarn Liewhiran [a] and Sukon Phanichphant* [e]

[a] Department of Physics and Materials Science, Faculty of Science, Chiang Mai University, Chiang Mai 50200, Thailand.

[b] Graduate School, Chiang Mai University, Chiang Mai 50200, Thailand.

[c] Department of Chemistry, Faculty of Science, Naraesuan University, Phitsanulok, 65000, Thailand.

[d] Nanoelectronics and MEMS Laboratory, National Electronics and Computer Technology Center, KlongLuang, Pathumthani 12120, Thailand.

[e] Materials Science Research Center, Faculty of Science, Chiang Mai University, Chiang Mai 50200, Thailand.

* Author for correspondence; e-mail: sphanichphant@yahoo.com

Received: 15 June 2017
Accepted: 14 September 2017

ABSTRACT

In this work, ethanol sensing films were prepared by spin-coating of PdO/WO_3 nanorods pasted onto Al_2O_3 substrates interdigitated with Au electrodes and tested towards 50-2000 ppm C_2H_5OH at different operating temperatures ranging from 150-350 °C. It was found that the C_2H_5OH responses of PdO-loaded WO_3 sensors monotonically increased with increasing operating temperature to 350 °C and increased greatly with increasing PdO-loading level up to 1.0 wt%. In particular, the optimal 1.0 wt% PdO-loaded sensor exhibited an ultra-high response of 1.52 $\times 10^4$ to 2000 ppm C_2H_5OH at 350 °C with a short response time of ~3 s. In addition, PdO-loaded WO_3 sensing films displayed high ethanol selectivity against CO, NO_2, NH_3 and H_2S. Therefore, PdO-loaded WO_3 nanorods sensors prepared by the precipitation and impregnation methods are promising for highly sensitive and selective for ethanol sensing.

Keywords: PdO/WO_3 nanorods, ethanol gas sensors

1. INTRODUCTION

Ethanol (C_2H_5OH) is a colorless liquid with a characteristic pleasant odor. A dilute aqueous solution of ethanol has a somewhat sweet flavor but it turns into a burning taste at a high ethanol concentration [1]. Ethanol can be conveniently detected in vapor phase due to its highly volatile nature and the detection of ethanol vapor is highly needed in various practical applications including the breath analysis for drunken driving identification and ethanol leak detection in industrial ethanol production lines. The ethanol detection range is typically 10-5000 ppm for monitoring of alcohol level in human blood and its threshold limit value (TLV) is 1000 ppm. In addition, ethanol vapor

may be detected near its explosive range of 3-19 vol% for safety concerns.

Gas sensors based on semiconducting metal oxides including SnO_2, WO_3, In_2O_3, TiO_2 and ZnO have been extensively used for the detections of various toxic pollutant gases, combustible gases and organic vapors. In general, their characteristics depend strongly on the chemical constituents as well as preparation condition, which define physical morphologies and chemical phases. In particular, the sensor properties in terms of response, response/recovery time and selectivity towards a specific gas can be boosted by activation with various additives, especially noble metals such as gold (Au), platinum (Pt) and palladium (Pd). Moreover, loadings with Au, Pt and Pd can substantially enhance the ethanol response of WO_3 nanostructures. Among these noble metals, Pd is attractive for practical gas-sensing applications due to its relatively low material price. The sensing performances of this composite material may be improved by synthesizing PdO/WO_3 nanostructures with larger specific surface area and better dispersion of Pd nanocatalysts using a more effective synthesis method. In this work, ethanol sensors fabricated from PdO/WO_3 nanorods as reported earlier [2] are presented.

2. MATERIALS AND METHODS

2.1 Preparation of Unloaded and PdO-loaded WO_3 Nanopowder and Characterization

Preparation of unloaded and PdO-loaded WO_3 nanopowder and characterization were reported earlier in Reference [2].

2.2 Sensing Film Fabrication and Characterization

Sensing films were fabricated by powder-pasting and spin-coating processes as reported earlier in Reference [2]. The sensors fabricated using P-0 and P-0.25Pd-P-2Pd (Pd = 0, 0.25-2.0 wt%) samples were assigned as S-0 and S-0.25Pd-S-2Pd, respectively.

2.3 Gas-sensing Measurement

The gas-sensing characteristics of metal oxide sensing films were characterized towards 50-2000 ppm C_2H_5OH, 2000 ppm NH_3, 2000 ppm CO, 10 ppm NO_2 and 10 ppm H_2S by the standard flow through technique. A flux of synthetic dry air as gas carrier was flowed to mix with the desired concentration of pollutants dispersed in synthetic dry air with a constant total flow rate of 2 L/min using a computer-controlled multi-channel mass flow controller. All measurements were performed in a temperature-stabilized sealed chamber at the ambient temperature of 25 °C while the sensor temperature was heated to different operating temperatures ranging from 150 °C to 350C by an external NiCr heater. The resistances of various sensors were continuously measured by voltage-amperometric technique with 1 V DC bias through a picoammeter with a built-in voltage source (Keithley 6487). The sensors were exposed to a gas sample for 10 min at each gas concentration and the air flux was then resumed for 25 min. The sensor response (S) is defined as the resistance ratio R_a/R_g [3, 4], where R_a is the stable resistance in dry air, and R_g is the steady-state resistance in a reducing gas including C_2H_5OH, H_2S, CO, and NH_3. The response definition is reversed for an oxidizing gas such as NO_2. The response time (t_{res}) is defined as the time required until 90% of the response signal is reached while the recovery time (t_{rec}) denotes the time needed until 90% of the original baseline signal is recovered.

3. RESULTS AND DISCUSSION

3.1 Gas Sensing Properties

The gas sensing properties of unloaded and PdO-loaded WO_3 nanorods are evaluated in terms of sensor response and response time as functions of operating temperature, gas concentration and PdO-loading level. Figure 1 shows the sensor response at various operating temperature ranging from 150 to 350 °C of unloaded and PdO-loaded WO_3 nanorods with different PdO-loading levels towards 2000 ppm C_2H_5OH in dry air. It is seen that the ethanol response of unloaded WO_3 sensor increases monotonically as the operating temperature increases from 150 to 350 °C. With PdO loading, the responses rise sharply as the operating temperature increases from 150 to 200 °C, then become almost steady as the temperature increases from 200 to 300 °C and increase quite rapidly again as the temperature increases further to 350 °C. Regarding the influence of PdO-loading level, the ethanol response increases greatly as the PdO- loading level increases from 0 to 0.25 wt% and then increases steadily as the PdO content increases from 0.25 to 1.0 wt% but becomes slightly decreasing as the loading content increases further to 2.0 wt%. In particular, the 1.0 wt% PdO-loaded WO_3 sensor (S-1Pd) exhibits the optimal response of ~1.52×10^4 to 2000 ppm C_2H_5OH at the highest working temperature of 350 °C. These results are consistent with some other reports [5], in which the sensor responses of WO_3 sensors are substantially improved with small amounts of PdO incorporation.

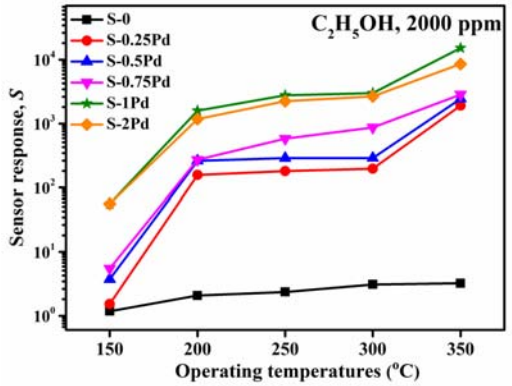

Figure 1. The sensor response vs. operating temperature of Pd-loaded WO_3 sensors with different Pd-loading levels (S-0, S-0.25Pd to S-2Pd) towards 2000 ppm C_2H_5OH.

The influence of PdO-loading level on the C_2H_5OH-sensing performances of WO_3 nanoparticles is further assessed at the operating temperature with the highest response (350 °C). Figure 2(a) demonstrates the change in resistance of WO_3 sensing films with different PdO-loading concentrations (S-0 and S-0.25Pd to S-2Pd) under exposure to various C_2H_5OH concentrations at 350 °C. It is seen that the baseline sensor resistance decreases initially with increasing PdO-loading level from 0 to 0.25 wt% (S-0 to S-0.25Pd) but then increases monotonically as the PdO-loading level increases further to 2.0 wt% (S-0.25Pd to S-2Pd). The dependence of sensor resistance with PdO-loading level will be analyzed in the next section. After C_2H_5OH exposure, every sensor exhibits a typical decrease of resistance in response to a reducing gas confirming the *n*-type semiconducting

behavior. Comparing the resistance changes among all sensors, it is seen that the resistance change of sensor tends to increase considerably with increasing PdO concentration from 0 to 1.0 wt% and the resistance change becomes slightly decreasing as the PdO content increases further to 2.0 wt%. Thus, the optimal PdO-loading level of WO_3-based sensors for C_2H_5OH sensing is 1.0 wt%. Moreover, it can be observed that the rate of change in resistance, response stabilization and baseline recovery of sensors are improved compared with those of unloaded one. Thus, the PdO-loaded WO_3 sensors can operate with better dynamic performances.

Figure 2(b) displays the corresponding sensing characteristics in terms of sensor response (solid line, left axis) and response time (dash line, right axis) of S-0 and S-0.25Pd to S-2Pd as a function of C_2H_5OH concentration at 350 °C. It is seen that the sensor response and response time improve quickly as PdO-loading level increases from 0 to 1.0 wt% but then slightly degrades when the PdO-loading concentration increases to 2.0 wt%. In particular, the S-1Pd sensor provides a high C_2H_5OH response ($S = 1.52 \times 10^4$ at 2,000 ppm) and relatively short response time (t_{res} = 3.02 s) compared with S-2Pd ($S = 8.59 \times 10^3$, t_{res} = 3.4 s), S-0.75Pd ($S = 2.86 \times 10^3$, t_{res} = 4.1 s), S-0.5Pd ($S = 2.56 \times 10^3$, t_{res} = 4.3 s), S-0.25Pd ($S = 1.92 \times 10^3$, t_{res} = 5.1 s) and S-0 (S = 2.67, t_{res} = 277 s). In addition, it still can detect C_2H_5OH at a low concentration of 50 ppm with a fair response of ~19.8. The attained response values are higher than some other C_2H_5OH sensors based on Pd-WO_3 materials, which exhibited sensor response only 1.76 to 20,000 ppm C_2H_5OH at 300 °C [5]. In addition, it is superior to some other reports of Au/Pt loaded WO_3 as well as SnO_2 sensors, which displayed high responses in the range of 1.8-1707 to 1000-2000 ppm C_2H_5OH as reported earlier [5-9]. However, it is inferior to the unloaded WO_3 sensor prepared by thick film screen printing that offered a high response of 1425 to 50 ppm ethanol but the reported sensor required a relatively high working temperature of 400 °C [10].

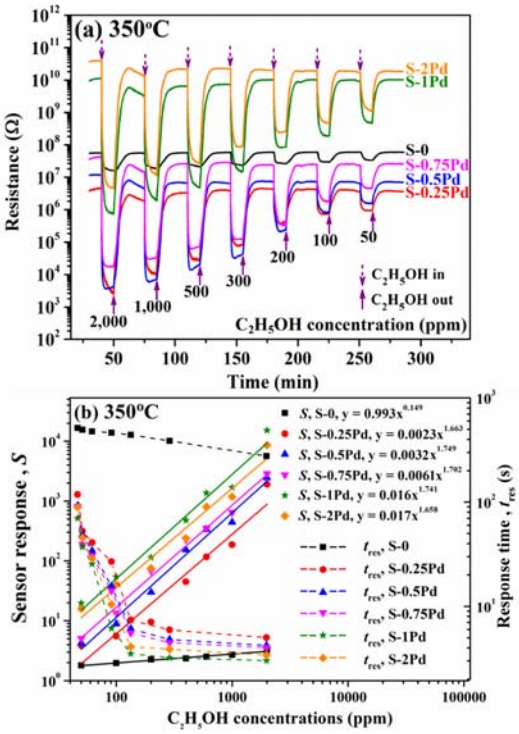

Figure 2. Change in resistance under exposure to various C_2H_5OH pulse with concentrations ranging from 50 to 2000 ppm of PdO-loaded WO_3 sensors with different PdO-loading levels (S-0, S-0.25Pd to S-2Pd) and (b) sensor response (solid line, left axis) and response time (dash line, right axis) vs. C_2H_5OH concentration of PdO-loaded WO_3 sensors with different PdO-loading levels (S-0, S-0.25Pd to S-2Pd) at 350 °C.

Regarding the gas concentration dependence, the sensor response characteristics of all sensors conform to the well-known power law equations as listed in the inset labels of Figure 2(b) while the

response times decrease rapidly with increasing C_2H_5OH concentration. In addition, the exponent values in the equations of unloaded sensor is close to 0.5 while those of PdO-loaded WO_3 sensors are near 1.5, implying a single and a triple gas-molecule interactions, respectively [11]. Moreover, it is found that Pd loading also results in considerable reduction of recovery time for the WO_3-based sensors. Based on the power-law fitting, the detection limit of the optimal sensor is estimated at a threshold response of 1.1 (resistance change of 10%) to be around 11 ppm [18], which is also better than several other previously reported several C_2H_5OH sensors [9, 17]. Thus, the PdO-loaded WO_3 nanorods prepared by the precipitation/impregnation methods is another promising alternative for highly sensitive detection of ethanol.

3.2 Selectivity of PdO/WO_3 Nanorods

The selectivity of unloaded and Pd-loaded WO_3 sensing films were assessed with 2000 ppm C_2H_5OH, 2000 ppm CO, 2000 ppm NH_3, 10 ppm NO_2 and 10 pm H_2S at 350 °C as displayed in Figure 3. It is seen that unloaded WO_3 nanorods still have similarly very low responses to all gases, showing very low ethanol selectivity. For PdO-loaded WO_3 nanorods, the C_2H_5OH response increases greatly with increasing PdO-loading level up to 1.0 wt% and then slightly decreases as the PdO content increases further to 2.0 wt% while the responses to other gases also increase with similar trends but the relative increments are still much lower than those of C_2H_5OH. Hence, the C_2H_5OH selectivity increases with increasing PdO-loading level and becomes optimal at the PdO content of 1.0 wt%. Therefore, the 1.0 wt% PdO-loaded WO_3 sensor exhibits not only very high response but also excellent ethanol selectivity against CO, NH_3, NO_2 and H_2S.

3.3 Gas-sensing Mechanisms

From overall results, Pd loading significantly influences the electrical resistance of WO_3 nanorods and the ethanol response is greatly enhanced by small amounts of Pd loading, which is optimal at the Pd-loading level of 1.0 wt%. The observations may be explained based on the formation of PdO-nanoparticles/WO_3-nanorods *p-n* heterojunctions by PdO nanoparticles on the WO_3 nanorods as illustrated in Figure 4. A hetero *p-n* junction system has been proposed to explain the enhanced gas sensitivity for PdO-WO_3 [12], NiO-SnO_2 [13] and CuO-ZnO [14] heterocontacts. The energy band structure diagram for *p*-type PdO/*n*-type WO_3 heterojunction is schematically depicted as shown in Figure 3(b). The oxygen-deficient WO_3 nanorods display *n*-type conductivity with electrons while oxygen-excess PdO nanoparticles show *p*-type conductivity with holes as charge carriers. When *p-n* heterojunction is formed at the interface between PdO nanoparticles and WO_3 nanorods, the electron transfer from n-type WO_3 nanorods and the hole transfer from p-type PdO nanoparticles will proceed until the system reaches the equalization of the Fermi level, leading to energy barriers in conduction and valence bands, depletion layers and increased electrical resistance. As a result, the baseline resistance of PdO-loaded WO_3 sensors tend to increase with increasing Pd-loading level.

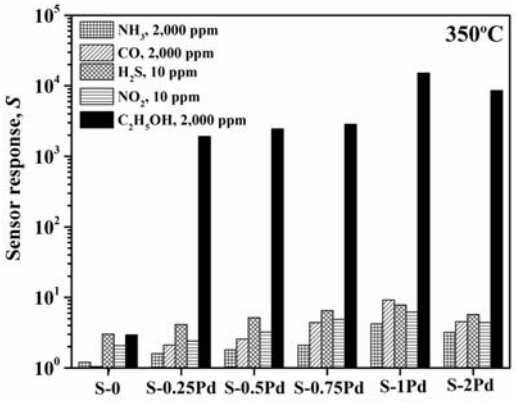

Figure 3. Selectivity histograms of sensor responses to 2000 ppm C_2H_5OH, 2000 ppm CO and 2000 ppm NH_3, 10 ppm NO_2 and 10 ppm H_2S of PdO-loaded WO_3 sensors with different PdO-loading levels (S-0, S-0.25Pd to S-2Pd) at 350 °C.

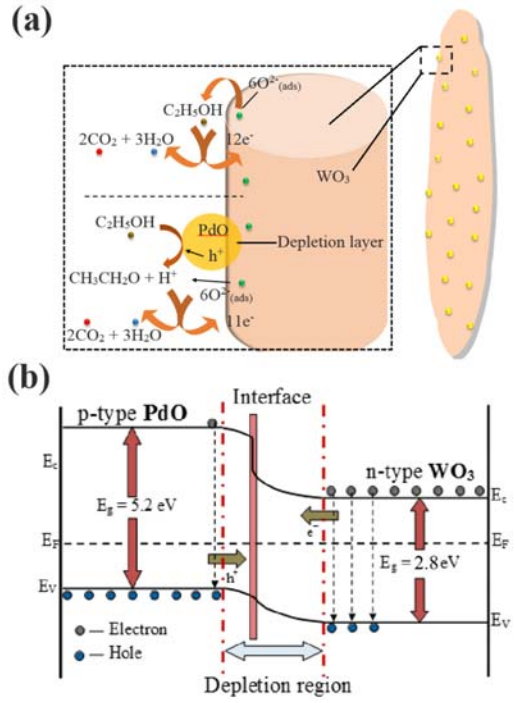

Figure 4. (a) Representative physical model for ethanol sensing mechanism at an interface between PdO nanoparticle and WO_3 nanorod and (b) energy band model of p-type PdO/ n-type WO_3 heterojunction. E_c: conduction band; E_F: Fermi level; E_v: valance band.

When exposed to ethanol, ethanol molecules will react with the preadsorbed oxygen species on the unloaded WO_3 surface according to the reactions:

$$O^- + e^- \rightarrow O^{2-} \qquad T > 300\ °C \qquad (1)$$

$$C_2H_5OH+6O^{2-} \rightarrow 2CO_2+3H_2O+12e^- \qquad (2)$$

From the reactions, the electrons will be released back to the WO_3 semiconductor leading to the reduction of surface depletion regions and electrical resistance of WO_3 nanoparticles. With the presence of *p*-type PdO, Pd^{2+} in PdO will react with hydroxyl ions on surface to form $Pd(OH)_2$ while holes interact with C_2H_5OH to form hydrocarbon intermediates and will react with preadsorbed oxygen species on the n-type WO_3 according to [12-14]:

$$Pd^{2+} \rightarrow 2OH^- \rightarrow Pd(OH)_2 \qquad (3)$$

$$C_2H_5OH+h^+ \rightarrow CH_3CH_2O+H^+ \qquad (4)$$

$$C_2H_5OH+H^++6O^{2-} \rightarrow 2CO_2+3H_2O+11e^- \qquad (5)$$

The reactions will result in the reduction of the potential barrier due to charge migration across the hetero interfaces. Thus, the addition of *p*-type PdO could enhance the ethanol adsorption kinetics and increase the sensitivity of the heterojunction sensor. This mechanism is supported by the previous study on bulk p-PdO/n-WO_3 heterocontacts, in which the electrical properties of the structural interfaces was shown to be extremely sensitive to the presence of adsorbed gas with a significant decrease of the sensor resistance upon gas exposure [7, 10]. Moreover, the nanoparticle/nanorod structures can enhance the sensor response via the increase of effective surface area for

gas interaction, leading relatively large gas-sensing enhancement compared with some other material structures [14, 16-17]. With increasing Pd loading concentration, the surface area of the hetero interfaces will increase, leading enhanced response. However, the surface area of the interfaces will reduce at a very high Pd loading concentration (>1 wt%) due to the agglomeration of PdO nanoparticles into larger particles.

4. CONCLUSIONS

In conclusion, unloaded WO_3 and PdO-loaded WO_3 (0.25-2.0 wt%) nanoparticles were synthesized by the modified precipitation /impregnation methods and characterized as reported earlier and systematically studied for ethanol sensing. PdO-loaded WO_3 nanostructures comprised 5-20 nm spherical or oval PdO nanoparticles dispersed over the surface of polycrystalline WO_3 nanorods. From gas-sensing data, the C_2H_5OH responses of PdO-loaded WO_3 sensors increased considerably with increasing the operating temperature up to 350 °C and enhanced greatly with increasing PdO-loading level up to 1.0 wt%. In particular, the optimal PdO-loaded sensor offered an ultra-high response of 1.52×10^4 to 2000 ppm C_2H_5OH at 350 °C with a short response time of ~3 s. Moreover, PdO-loaded WO_3 sensing films showed high ethanol selectivity against CO, NO_2, NH_3 and H_2S. Therefore, PdO-loaded WO_3 sensors prepared by the precipitation and impregnation methods are promising for highly sensitive and selective ethanol sensing.

ACKNOWLEDEMENTS

The authors gratefully acknowledge Center of Excellence in Materials Science and Materials Technology, the Graduate School, Department of Chemistry, Department of Physics and Materials Science, Faculty of Science, Chiang Mai University, Thailand, and National Electronics and Computer Technology Center, Pathumthani, Thailand.

REFERENCES

[1] Strang K., Ethanol: The Dose, Effects, and Side Effects of the World's Second Most Popular Drug (accessed 05.05.15).

[2] Kabcum S., Channei D., Tuantranont A., Wisitsoraat A., Liewhiran C. and Phanichphant S., *Sens. Actuators B*, 2016; **226**: 76-89. DOI 10.1016/j.snb.2015.11.120.

[3] Liewhiran C., Tamaekong N., Wisitsoraat A., Tuantranont A. and Phanichphant S., *Sens. Actuators B*, 2013; **176**: 893-905. DOI 10.1016/j.snb.2012.10.087.

[4] Huanga J., Xu X., Gu C., Wang W., Geng B., Sun Y. and Liu J., *Sens. Actuators B*, 2012; **173**: 599-606. DOI 10.1016/j.snb.2012.07.068.

[5] Li Y.X.X., Jian J. and Wang J., *Ceram. Int.*, 2010; **36**: 1917-1920. DOI 10.1016/j.ceramint.2010.03.016.

[6] Hubálek J., Malysz K., Prášek J., Vilanova X., Ivanov P., Lioobet E., Brezmes J., Correig X. and Svírák Z., *Sens. Actuators B*, 2004; **101**: 277-283. DOI 10.1016/j.snb.2004.01.015.

[7] Labidi A., Gillet E., Delamare R., Maaref M. and Aguir K., *Sens. Actuators B*, 2006; **120**: 338-345. DOI 10.1016/j.snb.2006.02.015.

[8] Srivastava V. and Jain K., *Sens. Actuators B*, 2008; **133**: 46-52. DOI 10.1016/j.snb.2008.01.066.

[9] Zhang J., Liu X., Xu M., Guo X., Wu S., Zhang S. and Wang S., *Sens. Actuators B*, 2010; **147**: 185-190. DOI 10.1016/j.snb.2010.03.017.

[10] Khadayate R.S., Waghulde R.B., Wankhede M.G., Sali J.V. and Patil P.P., *Bull. Mater. Sci.*, 2007; **30**: 129-133. DOI 10.1007/s12034-007-0023-8.

[11] Yamazoe N. and Shimanoe K., *Sens. Actuators B*, 2008; **128**: 566-573. DOI 10.1016/j.snb.2007.07.036.

[12] Annanouch F.E., Haddi Z., Ling M., Maggio F.D., Vallejos S., Vilic T., Zhu Y., Shujah T., Umek P., Bittencourt C., Blackman C. and Llobet E., *ACS Appl. Mater. Interf.*, 2016; **8**: 10413-10421. DOI 10.1021/acsami.6b00773.

[13] Guo Z., Chen G., Zeng G., Liu L. and Zhang C., *RSC Adv.*, 2015; **5**: 54793-54805. DOI 10.1039/C5RA10394K.

[14] Wangman D.D., Evans W.H., Parker V.B., Schumm R.H., Halow I., Bailey S.M., Churney K.L. and Nuttall R.L., *J. Phys. Chem. Ref. Data 11 (Suppl. 2)*, 1982. DOI 10.1063/1.555845.

[15] Chen Y., Yu L., Feng D., Zhuo M., Zhang M., Zhang E., Xu Z., Li Q. and Wang T., *Sens. Actuators B*, 2012; **166-167**: 61-67. DOI 10.1016/j.snb.2011.12.018.

[16] Singh S., Kaur H., Singh V.N., Jain K. and Senguttuvan T.D., *Sens. Actuators B*, 2012; **171-172**: 899-906. DOI 10.1016/j.snb.2012.06.002.

[17] Patil L.A., Shinde M.D., Bari A.R. and Deo V.V., *Curr. Appl. Phys.*, 2010; **10**: 1249-1254. DOI 10.1016/j.cap.2010.03.002.

[18] Yamazoe N. and Shimanoe K., *Sens. Actuators B*, 2008; **128**: 566-573. DOI 10.1016/j.snb.2007.07.036.